Advances and perspectives in tissue clearing using CLARITY

Kristian H. Reveles Jensen[1] & Rune W. Berg[2]

[1]krijen@sund.ku.dk, [2]runeb@sund.ku.dk
[1,2]University of Copenhagen
Blegdamsvej 3B
2200 Copenhagen
Denmark

May 23, 2017

Abstract

CLARITY is a tissue clearing method, which enables immunostaining and imaging of large volumes for 3D-reconstruction. The method was initially time-consuming, expensive and relied on electrophoresis to remove lipids to make the tissue transparent. Since then several improvements and simplifications have emerged, such as passive clearing (PACT) and methods to improve tissue staining. Here, we review advances and compare current applications with the aim of highlighting needed improvements as well as aiding selection of the specific protocol for use in future investigations.

Keywords:

CLARITY; tissue clearing; refractive index; brain; immunohistochemistry; microscopy

Chemical compounds:

Chemical compounds mentioned in this article: 1-Ethyl-3-(3-dimethylaminopropyl)carbodiimide (PubChem CID: 15908); 2,2'-Thiodiethanol (PubChem CID: 5447); α-Thioglycerol (PubChem CID: 7291); Acrylamide (PubChem CID: 6579); *D*-Sorbitol (PubChem CID: 5780); Diatrizoic acid (PubChem CID: 2140); Gylcerol (PubChem CID: 753); Iohexol (PubChem CID: 3730); Iomeprol-d3 (PubChem CID: 46781978); N,N,N',N'-Tetrakis(2-Hydroxypropyl)-ethylenediamine (amino alcohol, PubChem CID: 7615)

Introduction

The process of clearing tissue for the purpose of histological analysis has recently become a common tool in biological investigations. The purpose is to keep the proteins in a structure while removing the light-scattering lipids, and thus to allow deep penetration of light for fluorescent 3D microscopy. Several clearing methods have recently been developed.

Here, we focus on the advancement in the procedure called CLARITY (*C*lear *L*ipid-exchanged *A*crylamide-hybridized *R*igid *I*maging/Immunostaining/In situ-hybridization-compatible *T*issue-h*Y*drogel). It is a convenient histological fixation and clearing technique that enables immunohistochemistry (ICH) and maintenance of fluorophores during imaging of large volumes for 3D-reconstruction. The method was developed by Chung, Gradinaru, Deisseroth & colleagues and relies on the removal of lipids while keeping the protein and DNA of the tissue by creating a hydrogel by cross-linking with acrylamide (Chung et al., 2013; Chung and Deisseroth, 2013). Since then several improvements and simplifications have emerged, such as passive

clearing (PACT), and other adaptations (EDC-CLARITY).
We review advances, and compare current applications and limitations for this methodology, with the aim of highlighting needed improvements as well as aiding selection of the specific CLARITY or hydrogel-based protocol for use in future investigations. CLARITY was originally demonstrated on rodent brains but has since been successfully applied to other tissues organs and species, e.g. fish and plants. In this review, we primarily focus on nervous tissue although the protocols work for other tissues as well.

The original CLARITY method

CLARITY works by polymerising proteins, DNA, and RNA in fixed tissue using acrylamide to form a tissue-hydrogel hybrid before lipid-removal. The acrylamide based hydrogel binds molecules with amine ends, predominantly proteins and a small proportion of DNA and RNA, into a skeleton structure, which is permeable to larger molecules. The lipids are then encapsulated into micelles using detergent (sodium dodecyl sulfate, SDS). The micelles are electrically charged and can therefore easily be carried out through the pores by an applied electrical field. Antibodies for immunohistochemistry (ICH) can also penetrate the hydrogel to reach and stain the fixed membrane proteins. The original protocol was first demonstrated on whole adult mice brains and can be summarised in the following steps:

1. **Fixation of tissue.** The animal is transcardially perfused with a mixture of 4% (w/v) paraformaldehyde (PFA), 4% (w/v) acrylamide, 0.05% (w/v) bis-acrylamide, 0.25% (w/v) VA-044 and in phosphate-buffered saline (PBS), and the brain is removed and incubated in the same solution for 3 days.
2. **Hydrogel formation.** A 3-hour heat activation at 37°C for the thermal initiator, VA-044, results in the polymerisation of the acrylamide and bis-acrylamide to the PFA-fixed tissue.
3. **Lipid extraction.** Tissue clearing, or lipid removal, is accomplished by incubating the tissue in a sodium borate buffer (0.2 M, pH 8.5) containing 4% (w/v) SDS in a custom-designed electrophoretic chamber. The basic pH leads to negatively charged micelles, which pass trough the porous hydrogel by electrophoresis using a 10-60 V current applied across the sample at 37-50°C for two days.
4. **Refractive index matching.** The tissue is washed in PBS for two days to remove SDS. The tissue-hydrogel has a refractive index (RI) of 1.44-1.46. The tissue is incubated with a proprietary imaging solution, FocusClear (CelExplorer Labs Co.), with a similar RI of 1.454 to increase transparency.

The novelty in the CLARITY method is the second step since utilization of a hydrogel had a clear benefit compared with other methods. Even using the harsh 4% SDS for a week, the cleared tissue had only 8% protein loss. For comparison, in PFA-fixed tissue in 4% SDS, without the hydrogel up to 65% protein was lost. Similar protein loss is observed using other clearing methods without a hydrogel, such as Sca/e, which uses urea and glycerol (Hama et al., 2011). The effective retention of proteins and antigens also enabled repetitive staining, where antibodies could be washed out briefly in 4% SDS and restained.
However, the step of lipid extraction had several limitations: active clearing with electrophoresis required a custom-designed chamber with a continuous exchange of SDS solution. The electrical current, if not properly controlled, can decompose or discolour the tissue. Thus, since the original CLARITY method both required expensive elements in step 4 such as the RIMS medium (FocusClear) and was difficult to implement, a potential for improvement presented itself. Several labs have employed a more simple version of CLARITY without electrophoresis, which is the passive CLARITY clearing. The need for cheaper refractive index imaging solutions than the original (FocusClear) has also become apparent. First, we will address the general challenges in tissue clearing.

> “
>
> CLARITY in its original form used electrophoretic tissue clearing (ETC) to extract lipids from large samples, which can be challenging to implement and can cause variability in final tissue quality, including epitope loss, damage to fine processes, and tissue browning due to heating (Lee et al., 2014).

General challenges

There are several issues to consider when clearing tissue. Processing time, the number of procedural steps, the toxicity of reagents, signal and bleaching of fluorophores and the required concentration of primary and secondary antibodies, which are usually expensive and therefore beneficial to reduce. Efficiency in the extraction of lipids from the hydrogel, i.e. how much of the original lipids remain and how much time does the procedure require. Successful extraction of lipids is usually manifested in the transparency of the sample and the incubation time is often adjusted by the investigator for the sample to achieve the appropriate properties. Although the tissue transparency has been attributed to the removal of lipids during the procedure, it is still unknown to what extent the lipids are cleared from the sample and how much remains in transparent samples. This is contrary to the degree of protein loss, which has been quantified (Chung et al., 2013; Lai et al., 2016).

A major challenge introduced by clarified tissue samples is the imaging technology followed by the data analysis. Using conventional single photon laser scanning confocal microscopy, vast areas of the sample become unnecessarily illuminated, which introduces photobleaching of the fluorophores as a general issue. Photo-bleaching is potentially devastating in samples with a weak fluorescent signal, such as in Brainbow tissue (Cai et al., 2013).

For the same reason, it is important to limit the protein loss during storage of CLARITY samples. A novel imaging technology overcomes this issue by selectively only illuminating a single thin plane in a sequential manner. This technique is known as light-sheet microscopy, which can give a high rate of data acquisition of high contrast and resolution, and with very limited exposure to the rest of the sample (Stefaniuk et al., 2016). Light-sheet microscopy is remarkably faster than traditional single- or two-photon laser scanning microscopy. Several variants of light-sheet microscopy are commercially available, but they are not inexpensive and will represent a major investment to most laboratories. Another issue to consider is the price of the equipment and protocol compounds. The equipment necessary to set up active CLARITY with electrophoresis is approximately $6,800. FocusClear is the originally recommended imaging media, which is expensive, but other less expensive alternative exist such as RIMS, sRIMS and glycerol.

It is also important to consider that acrylamide, the primary component in the formation of the hydrogel, is a carcinogenic compound and is on the U.S. federally regulated list of 'extremely hazardous substances'. Finding a less toxic alternative is therefore appealing. An acrylamide-free procedure with fewer steps has been suggested that the SDS alone can extract the lipids without the need for the toxic hydrogel (Lai et al., 2016).

Improvements in the CLARITY protocol are described below regarding each step below. Modifying elements in the CLARITY protocol such as price, labour-intensity and toxicity are worth considering for optimisation.

Variants and improvements of CLARITY

The steps of the CLARITY procedure including staining and imaging is summarized as follows: 1) Tissue fixation and cutting, 2) Hydrogel polymerization, 3) Passive or active lipid removal, 4) Staining, 5) Optical clearing, 6) Imaging (**figure 1**). Here we summarize the improvements in these steps. A list of variants of the CLARITY improvements are found in **table 3**.

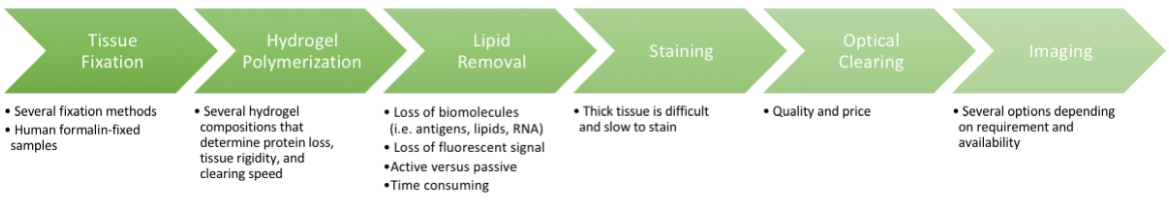

Figure 1: **Steps in the CLARITY procedure including challenges and considerations.**

1. Tissue fixation and cutting

Tissue fixation is the initial step in practically all histology as well as CLARITY. The original protocol prescribes the animal to be transcardially perfused with 4% PFA together with the acrylamide monomers and activator VA-044, and the nervous tissue further incubated in the same solution for 3 days (Chung et al., 2013). In the following published protocol, the incubation was shortened to 1 day (Tomer et al., 2014). However, fixation with 4% PFA alone was later demonstrated as sufficient for the subsequent cross-linking and hydrogel polymerization if the tissue was just incubated in the monomer solution afterwards (Costantini et al., 2015; Lee et al., 2014; Zheng and Rinaman, 2016; Jensen and Berg, 2016).
Transcardial perfusion of PBS to remove blood followed by the fixative or monomer solution is preferable. However, for some purposes just fixing the excised tissue, which has not been perfused e.g. human tissue, overnight in 4% PFA in PBS is sufficient.
Trimming the tissue down to the minimal required volume speeds up clearing and staining. Smaller tissue volume also results in less light scattering and clearer imaging. This can be done by embedding the tissue in low melting agar and cutting the tissue down to the most practical form e.g. a hemisphere, 1-2 mm slices or sections on a vibratome. Slicing the tissue after the hydrogel formation (step 2) is not recommended since the hydrogel swells to a sticky mass and is difficult to cut accurately, besides being carcinogenic. We recommend cutting before incubation and the polymerisation step.

2. Hydrogel polymerization and composition

Warning! Acrylamide is carcinogenic and should be handled with great care. After fixation, the tissue needs to be cross-linked and hybridised into a hydrogel by the acrylamide monomers to stabilise biomolecules and retain them during tissue clearing. The purpose is to achieve a fast and homogeneous clearing process, with good antibody penetration depth and retaining the desired antigens (protein). PFA fixes the tissue and supposedly acts as an anchor point for the acrylamide monomers to polymerise into a mesh. After removal of lipids the proteins are left in a hydrogel (step 3).
The original hydrogel monomer solution (4% PFA, 4% acrylamide, 0.05% bis-acrylamide) was optimized to provide a balance between hydrogel rigidity and porosity with minimal protein loss (∼8% when cleared in a 4% SDS borate buffer) after ETC clearing (Chung et al., 2013). However, solution adjustments may be useful for applying CLARITY to certain kinds of tissues and passive and active clearing.
While an emphasis has been put on optimising the hydrogel composition for passive clearing, the modifications in the hydrogel composition are applicable to both passive and active clearing by electrophoresis. The hydrogel presented in the PACT method (the A4P0 composition) is the current default in for passive clearing, but it is also applied in active clearing with the ACT-PRESTO protocol. Others have used 2%PFA and 2% acrylamide for active clearing (Bastrup and Larsen, 2017). The variations in the hydrogel monomer solution are therefore presented here before addressing the lipid extraction step.

PACT and PARS

Yang et al. (2014) focused on developing a simple version of CLARITY based purely on the passive removal of lipids, i.e. passive clearing. They tested several hydrogel compositions and SDS concentrations leading to an improved protocol named PACT (*pa*ssive *C*LARITY *t*echnique) protocol. They had three main findings: First, omitting PFA in the monomer solution did not change the degree of protein loss, but did increase IgG penetration depth i.e. better antibody labelling. Second, omitting PFA leads to faster transparency, but also a greater tissue swelling (∼230%), yet the swelling is transient, and may improve staining by making the tissue more porous. Finally, lower acrylamide concentration (i.e. 2%) leads to less cross-linking and less solid tissue, this in turns results in faster clearing, but also greater tissue swelling and protein loss. Hence, they concluded that 4% acrylamide, which they referred to as A4P0 solution, is optimal for nervous tissue and other tissues e.g. liver and kidney.
While A4P0 was optimised for passive clearing, the recipe is also used in active clearing (Lee et al., 2016). Rather than tissue incubation in the monomer solutions, the PACT reagents can be delivered either via the vasculature (intracardial injection) or intracranially by injection into the cisterna magna or a subdural

cannula above the olfactory bulb to achieve whole body or CNS clearing and labelling. The technique is termed PARS (*P*erfusion-assisted *A*gent *R*elease in *S*itu). The PACT reagents used in PARS are recirculated into the cerebrospinal fluid (CSF) or through the whole-body vasculature for several days-to-weeks in closed-loop perfusion system mimicking regular blood flow allowing for clearing and staining deep in the tissue (Tomer et al., 2014). But PARS does not change the speed of tissue clearing of the brain or internal organs (Woo et al., 2016), **table 2**. The PARS delivery system can be combined with other of the below methods if needed. In, summary, PACT/PARS is a radical improvement since they provide a simpler recipe, which also gives a faster clearing with better antibody staining.

psPACT

psPACT (*processes separate* PACT) enhanced the clearing speed by splitting the monomer incubation into *separate processes* before polymerisation: an initial 24 hr incubation at 37C in acrylamide solution (4% w/v in PBS), then a 6-12 hr incubation at room temperature in VA-044 initiator solution (0.25% w/v in PBS) for the hydrogel formation, which shortens the subsequent clearing time with ∼10% (Woo et al., 2016); however there are no comparisons of protein loss.

ePACT

ePACT (*expansion-enhanced* PACT) is used to expand thin tissue sections (100μm) to larger volumes for better resolution and resolution beyond the diffraction limit (Treweek et al., 2015). The hydrogel is composed of an acrylate-acrylamide copolymer and cleared with 10% SDS (ICH is done prior) and then digested with collagenase before incubation in water leading to water absorption and tissue expansion.

FASTClear

In CLARITY protocols proteins are assumed to be fixed to an acrylamide scaffold via PFA, while lipids are washed out by the amphiphilic SDS-micelles. Nevertheless, Lai et al. (2016) demonstrated an acrylamide-free version of CLARITY (i.e. essentially only washing with SDS followed by RIMS) gave better results for formalin-fixed tissue, while also arguing that the tissue-PFA-acrylamide cross-linking is only theoretical and does not actually occur, thus omitting acrylamide-polymerisation is not only easier but also better. Therefore, they developed a Free of acrylamide SDS-based tissue-clearing (FASTClear) protocol (Liu et al., 2016).

Other modifications

It is worth noting that the PACT protocol also omits bis-acrylamide, which acts as a secondary cross-linker, thus does not link to PFA-tagged biomolecules, but directly cross-links poly-acrylamide chains to form the gel. Therefore Bis-acrylamide increases the rigidity of the hydrogel network by creating cross-links inside cavities that may be void or sparse of biomolecules such as the ventricles. Bis-acrylamide also causes all the hydrogel solution surrounding the tissue sample to cross-link and form a gel during the polymerization step, which is a helpful aid in determining successful polymerisation. The surrounding gel can easily be manually removed from the tissue via physical rubbing/handling.

Without bis-acrylamide and the gel formation outside the tissue, the sample can simply be removed from the solution following the polymerization step and is therefore recommended for small or fragile specimens that cannot withstand the physical gel removal process.

The incubation time of the tissue in the monomer solution before polymerisation varies among authors with 1-3 days of incubation for a whole rodent brain, while for 1-2 mm slices overnight is sufficient.

Saponin is a mild non-ionic surfactant often used to permeabilise cellular membranes in conventional histology. It was briefly mentioned by Chung and Deisseroth (2013) as an adjunct in the monomer solution to improve diffusion of the hydrogel monomer and initiator into tissues, where cardiac perfusion is not possible e.g. post-mortem human tissues and zebrafish brains. Saponin reportedly shortens the incubation time required in the hydrogel monomer infusion process. However, saponin may cause bubbles, and therefore it is not recommended and has not since been reported utilised. In zebrafish adding dimethyl sulfoxide (DMSO) improves monomer penetration.

Another challenge for users has been initiating the polymerisation, which is inhibited by oxygen. The original

CLARITY protocol, therefore, involved a vacuum desiccation chamber(Chung et al., 2013). While Yang et al. (2014) demonstrated, it was sufficient to displace the oxygen from the solution by bubbling for ∼10 min with Nitrogen before initiation. Some users have found it sufficient to prevent aeration by sealing the monomer solution off by placing a layer of vegetable oil on top in the test tube (`forum.claritytechniques.org`), others that the tube can also simply be filled entirely with the monomer solution to minimise inhibitory effects of the oxygen (Bastrup and Larsen, 2017). Another method is to simply double the concentration of the initiator, VA-044, which eliminates any vacuum purging or nitrogen backfilling. This method is called 'simplified CLARITY method' (or SCM), but was only tested on thin sections, of 100 μm (Sung et al., 2016).

3. Lipid removal

Since membrane lipids are the main cause of light diffraction in tissues and comprise ∼60% of nervous tissue, lipid elution renders the tissue translucent. Temperature and solutions affect lipid clearing: speed, uniformity and protein loss. The original CLARITY protocol used a 4% SDS (sodium borate buffer, pH 8.5) intended for active clearing by electrophoresis (see below). Tissue clearing can be *passive* where lipids captured in detergent micelles slowly diffuse out of the tissue into the wash solution or *active* at an accelerated rate by employing strong electronic forces, **figure 2**. In a study comparing active and passive CLARITY, there were no significant differences in protein concentration as an effect of active versus passive clearing (Epp et al., 2015).

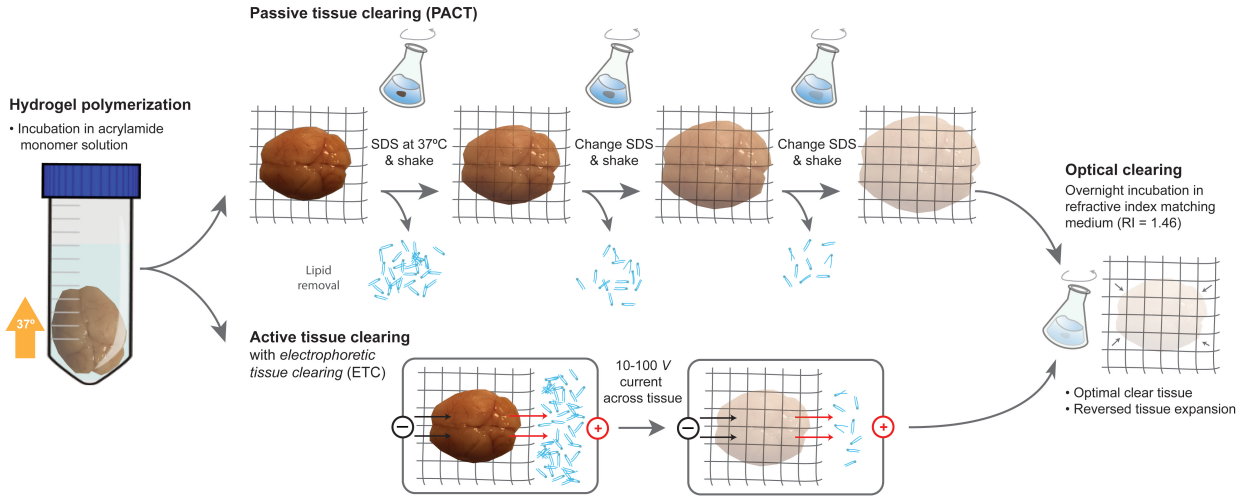

Figure 2: **CLARITY tissue clearing: passive and active.**
The hydrogel-tissue hybrid is formed (left) by an incubation in the acrylamide monomer solution with the initiator VA-044. Polymerization is activated by heat. Afterwards, the lipids can either be cleared from the tissue by passive (top) or active (bottom) methods. The detergent, SDS, collects lipids and carries them out of the tissue leaving behind a transparent hydrogel-tissue hybrid. Passive tissue clearing, PACT (top), is straightforward and inexpensive, but also a slower process as it relies on diffusion, which is enhanced by gentle shaking and an elevation of temperature. During this process the tissue absorbs water and expands in volume up to ∼200%, which improves the access of antibodies and thus the staining. The swelling is reversed in the hygroscopic medium (right). The alternative method of tissue clearing requires more equipment and supervision as it uses electrophoresis (bottom). The negatively charged lipid micelles are actively carried by the electrical field, which greatly enhance the extraction rate. In the final step of optically clearing the tissue (right) the hydrogel is incubated overnight in a refractive index matching medium to complete transparency.

Passive lipid removal

Passive clearing without electrophoresis is gentle on the tissue with little risk of damage apart from longer clearing, which can reduce the signal from fluorescent proteins and increase the loss of biomolecules. It is inexpensive and requires little equipment. A simplified diffusion-based method omitting the electrophoretic chamber, coined CLARITY2, to clarify <1.5 mm thick slices was proposed by Poguzhelskaya et al. (2014) .

PACT

Yang et al. (2014) optimised the hydrogel composition for passive clearing and also tested several SDS concentrations leading to the improved PACT protocol. They found that 8% SDS (in PBS buffer, pH 7.5) gave a faster and more uniform tissue clearing compared to 4% SDS, 20% SDS and 10% sodium deoxycholate. For this reason, PACT has become the default passive CLARITY protocol. There is no significant difference in the swelling and shrinking behaviour of passively cleared rodent gut tissue with CLARITY or PACT solution, nor a difference in clearing time (Neckel et al., 2016).

mPACT

Woo et al. (2016) added 0.5% α-thioglycerol (inspired by the SeeDB method (Ke et al., 2013)) to the PACT clearing solution, which improved clearing time with ∼10%, and named it psPACT with added α-thioglycerol mPACT (*modified* PACT), which gave a combined ∼25% faster clearing compared with regular PACT on most tissues, **table 2**). Although the effect of α-thioglycerol on protein loss has not been reported, it is unlikely that it has an adverse effect. On the contrary, since α-thioglycerol preserves proteins by counteracting the Maillard reaction, i.e. browning of the specimen, autofluorescence and antigen loss is likely to be minimal.

Temperature and speed

Tissue clearing is often performed at room temperature (RT) or 37°C. Generally, increasing temperature accelerates clearing and imaging depths but at the risk of damage to the tissue and quenching fluorescent proteins. Passively clearing 1 mm cortical sections takes ∼48 hours at 37°C compared to ∼12 hours at 57°C (Yu et al., 2017) Nonetheless, Yu et al. (2017) found that an elevated temperature range of 42-47°C for PACT resulted in faster transparency and deeper imaging depth than 37°C while having a comparable fluorescence preservation. There is reportedly no significant difference in protein loss temperature as high as 55°C compared to 37°C (Epp et al., 2015).

Passive clearing can be improved by gentle shaking, continuously replacing the clearing solution (**Figure 2**) or with a flow-assisted clearing setup with a circulator. An alternative setup without a circulator is using a 50 ml conical tube perforated with several holes at the 15-20 ml mark and at the bottom of the tube, which is inserted into a 250 ml glass bottle filled with clearing solution. Unidirectional flow is created by using a magnetic stir bar on a stirring hot plate to accelerate the clearing at the desired temperature (`capture-clarity.org/optimized-clarity`). The clearing time of various tissues depending on protocol are displayed in **table 2**.

Active lipid removal by electrophoresis

The tissue is composed of different types of lipids primarily fatty acids and phospholipids. The detergent, SDS, captures the lipids in SDS micelles. The micelles are negatively charged at basic pH (7.5–8.5) and carries the lipids along the electric field. This electrophoretic tissue-clearing (ETC) enhances the speed of extraction by orders of magnitude such that a large tissue sample e.g. a mouse brain becomes transparent a matter of hours to days instead of days to weeks during passive clearing (Tomer et al., 2014). Lipid clearing using ETC is faster and therefore results in less tissue swelling compared with passive clearing.

The ECT system should have three elements: 1) The chamber containing the sample and electrodes. 2) A circulator, which controls flow rate and temperature. This can be a simple pump and a liquid reservoir that serves to remove electrophoretic by-products such as acid, bubbles and heat. 3) A buffer filter to filter out larger particles in the clearing solution.

There are, however, important caveats to consider when using ETC. If the electrical field is too strong, small bubbles form inside the hydrogel that make the hydrogel opaque, while bigger bubbles may rupture hydrogel

(Kim et al., 2015). Keeping the voltage small enough to avoid this issue, ETC is a helpful step in clearing the sample. The electric field is recommended to be applied as a low–voltage constant current generator of 250-280 mA to ensure low voltage field (10-40 V). Such a field will avoid electrolysis of water in the liquid and formation of bubbles (Lee et al., 2014). Running ETC at higher temperatures (55°C) produces very clear tissue, but the tissue tends to lose structural integrity (Epp et al., 2015). Lower the clearing temperature ∼15°C to counteract Joule–heating is also recommended (Kim et al., 2015). Practically the tissue sample is placed in a custom-designed electrophoretic chamber with platinum electrodes as well as drainage and access of liquid (Tomer et al., 2014; Lee et al., 2016). The original CLARITY chamber had wire electrodes with a surface area of 314mm^2, which could clear a mouse brain in 5-16 days, whereas electrode plates with a greater surface area of 1200mm^2 as in ACT gives faster clearing (whole mouse brain and other organs within 24 hrs, **table 2**) and less tissue damage (Lee et al., 2016).

Another caveat of ECT is the flux of lipids is in one direction along the field, which means that the central parts, as well as the parts along borders in parallel with the field, will not have extraction lipids in the same degree as the perpendicular parts. This results in a non-even extraction and penetration of antibodies when using ECT for ICH. A solution to this problem is, rather than using a static field, to change the direction of the electric field over time, e.g. by rotating the direction. Such rotational electrical field enhances the stochastic electro-diffusion, which enhances lipid extraction as well as staining of large and dense tissue with nuclei dyes, proteins, antibodies (Kim et al., 2015). The two-chamber design with the rotational electrical field can clear mice brains and other organs within 3 days (**table 2**).

While most chamber designs are freely and commercially available, setting up ETC is expensive, but 3D printing of shared designs may significantly reduces costs for experimenters and allow for organ-specific designs (Sulkin et al., 2013). An overview of the three ECT approaches and where to find free designs and commercial ETC chambers are summarised (**table 1**).

Table 1: **ETC protocols and chambers for active lipid removal.**
CLARITY and ACT are use a sodium borate buffer, while the stocastic eltroctransport uses a sodium borate buffer with lithium hydroxide and a two-chamber system. *The Stocastic Electrotransport system can also be used to rapidly deliver dyes or antibodies into the tissue during staining.

Protocol	Electrodes and field	Speed and tissue damage	Time to clear a mouse brain	Freely available protocol and chamber blueprints	Commercial options
CLARITY	Wire-electrodes; unidirectional field (10-30 V;280mA)	(+) Linear with V Discolouration and tissue damage	15–16 days	Chung et al. (2013); Tomer et al. (2014) Bastrup and Larsen (2017) `wiki.claritytechniques.org`	
ACT	Large sufrace plate-electrodes; unidirectional field (1.5A)	(+++) Linear with V Less tissue damage	6 hours	Lee et al. (2016)	X-CLARITY (Logos Biosystems)
*Stochastic Electrotransport**	Wire-electrodes; rotating field (10-100 V)	(++) Quadratic with V Least tissue damage	3 days	Sylwestrak et al. (2016) and `www.chunglabresources.com`	SmartClear I & II (LifeCanvas Tech)

Loss of fluorescent proteins and antigens

Many investigations employ transgenic rodents expressing fluorescent proteins such as GFP or YFP in a specific neuronal population e.g. dopaminergic neurons or parva-albuminergic neurons. To target subpopulations or specific pathways, viral tracers are similarly used to induce fluorescent protein expression in specific neuronal populations. However, the fluorescent proteins are vulnerable to over-fixation, denaturation and elution with subsequent signal loss and may require optimisation. In 1 mm brain slices with genetically expressed GFP, when cleared by passive CLARITY, tissue transparency reaches a plateau after 5 days, while the fraction of GFP remaining in the tissue decreases rapidly during clearing (Magliaro et al., 2016), demonstrating a trade-off between transparency and protein retention. Antigens and fluorescent proteins are lost during tissue clearing. The optimal clearing is the shortest duration with the best ratio of transparency and protein retention. Magliaro et al. (2016) measured transparency with a regular digital camera and they measured antigen and fluorescent protein loss into the clearing solution with a fluorescent plate reader or a spectrophotometer.

Table 2: **Clearing times for various organs and tissues with different methods.** Using PARS in conjunction with PACT or mPACT i.e. PARS-PACT and PARS-mPACT did not change clearing time compared to PACT and mPACT(Woo et al., 2016). However, the authors of each study likely have different definitions of when a tissue is sufficiently transparent e.g. regarding mice intestine. Organs are whole unless otherwise noted. *A: acrylamide, B: bis-acrylamide

Animal	Organ	Size	Clearing Protocol	Clearing time (days)	Reference
Mice	**Brain**	1 *mm*	ACT	2 *hrs*	Lee et al. (2016)
		1 *mm*	PACT (4% A, 0.05% B)	4	Jensen and Berg (2016)
		2 *mm*	Active CLARITY (2% PFA, 2% A)	2	Bastrup and Larsen (2017)
		3 *mm*	ACT	4 *hrs*	Lee et al. (2016)
		3 *mm*	Active CLARITY	3	Lee et al. (2014)
		whole	ACT	6 *hrs*	Lee et al. (2014)
		whole	Stocastic Electrotransport	3	Kim et al. (2015)
		whole	Active CLARITY (4 d at 37°C, 1 d at 55°C)	5	Epp et al. (2015)
		whole	Active CLARITY	12–16	Lee et al. (2014)
	Brain & spinal cord	whole	mPACT	14	Woo et al. (2016)
		whole	PACT	23	Woo et al. (2016)
	Bone		Bone CLARITY	21	Greenbaum et al. (2017)
	Embryos		mPACT	3	Woo et al. (2016)
	Heart		mPACT	15	Woo et al. (2016)
			Stocastic Electrotransport	3	Kim et al. (2015)
	Intestine		ACT	3 *hrs*	Lee et al. (2014)
			Active CLARITY	8–12	Lee et al. (2014)
			Passive CLARITY	12–14	Neckel et al. (2016)
			PACT	12–14	Neckel et al. (2016)
			mPACT	15	Woo et al. (2016)
			PACT	21	Woo et al. (2016)
			Stocastic Electrotransport	1	Kim et al. (2015)
	Kidney		ACT	1	Lee et al. (2016)
			Active CLARITY	8–12	Lee et al. (2014)
			Stocastic Electrotransport	3	Kim et al. (2015)
	Liver		ACT	1	Lee et al. (2016)
			Active CLARITY	18–22	Lee et al. (2014)
			PACT	22	Woo et al. (2016)
	Lung		ACT	5 hrs	Lee et al. (2016)
			Active CLARITY	13–17	Lee et al. (2014)
			mPACT	14	Woo et al. (2016)
			PACT	18	Woo et al. (2016)
			Stocastic Electrotransport	3	Kim et al. (2015)
	Pancreas		Active CLARITY	8–12	Lee et al. (2014)
			mPACT	17	Woo et al. (2016)
			PACT	17	Woo et al. (2016)
Rat	**Brain**	hemisphere	ACT	8 *hrs*	Lee et al. (2016)
		4 *mm*	mPACT	5	Woo et al. (2016)
		4 *mm*	psPACT	7	Woo et al. (2016)
		4 *mm*	PACT	10	Woo et al. (2016)
	Spinal cord section	4 *mm*	PACT (4% A, 0.05% B)	6	Jensen and Berg (2016)
	Brain & spinal cord	whole	mPACT or PARS-mPACT	21	Woo et al. (2016)
	Heart		PARS-mPACT	16	Woo et al. (2016)
	Kidney		mPACT or PARS-mPACT	23	Woo et al. (2016)
			PARS-PACT	23	Woo et al. (2016)
	Liver		PARS-mPACT	23	Woo et al. (2016)
	Lung		PARS-mPACT	18	Woo et al. (2016)
	Pancreas		mPACT or PARS-mPACT	15	Woo et al. (2016)
	Spleen		mPACT or PARS-mPACT	19	Woo et al. (2016)
Zebrafish	**Whole adult fish**		ACT	6 *hrs*	Lee et al. (2016)
			PACT (1% A, 0.05% B)	5	Cronan et al. (2015)
			PACT (4% A, 0.05% B)	30+	Cronan et al. (2015)

4. Staining

The main feature of CLARITY is the ability to combine large volume tissue clearing with molecular phenotyping by ICH and other staining methods. Multiple rounds of staining are possible without damage to the preserved structure since the innate biomolecules are chemically bound in the tissue-hydrogel. The tissue clearing solution containing detergent (SDS) can be used to denature antibodies, disrupt binding, and wash antibodies and other molecular labels out of the hydrogel-embedded tissue as preparation for addition rounds of staining. The procedure is simply: incubate overnight with shaking in PBST at 20-40°C, then incubate overnight with shaking in clearing solution at 60°C to wash out antibodies, finally incubate overnight with shaking in PBST at 20-40°C to wash out SDS before next round of ICH and imaging (Tomer et al., 2014). However, there were several limitations e.g. slow staining, incompatible with lipid dyes and poor retention of RNA that have been improved upon.

Passive versus active staining

Similar to the clearing of lipids, the application of antibodies for IHC can be performed either passively by diffusion or actively with the assistance of an electrical field or other means. Two of the main challenges in staining is uniformity and depth, together with the speed of staining relying on diffusion. The slow rate of penetration of antibodies within the hydrogel is a significant limiting factor in many experiments, as thick tissues require weeks to months to adequately label. Increasing the pore size of the hydrogel (by reducing acrylamide concentration) had limited effect. Diffusion speed is dependent on the molecular weight of the dye or antibody. By staining thick CLARITY-treated tissue with the small molecule, DAPI (0.28 kDa) can be done reliably overnight (Jensen and Berg, 2016), whereas staining antibodies (150 kDa) takes several days to weeks. The time of penetration using diffusion can be reduced by half by using smaller antibody fragments (such as $F(ab')_2$ (110 kDa) and Fab (50kDa)) (Li et al., 2015).

Another approach to improve antibody staining is using high antibody concentrations or two primary antibodies for a single target, which improved staining speed and quality of parvalbumin-expressing neurons (Bastrup and Larsen, 2017).

The PARS method to clear the tissue can also be used as an active staining method where the staining solution is delivered via the vasculature route mimicking blood flow to reach the whole body and all areas of the tissues to increase speed and penetration depth. If only staining of the brain or CNS is desired delivery by a subdural cannulation directly above the olfactory bulb or in the cisterna magna is more effective.

An initial report demonstrated how an electrophoretically-driven approach could decrease the delivery time of antibodies by taking advantage of their net charge. A static and unidirectional $25\,V$ electric field increased antibody penetration by more than 800-fold compared to simple diffusion (Li et al., 2015).

Kim et al. (2015) found that static electrophoresis resulted in substantial tissue damage, similar to the problems with ETC when clearing lipids (see above). The strategy proposed by the Chung group is based on *stochastic electrotransport*. A rotational electric field selectively dispersed charged molecules without interfering with the endogenous biomolecules. Molecules of different sizes (70-2,000 kDa) benefited from stochastic electrotransport and gave rapid homogeneous staining of whole brains by fluorescent dyes, proteins, and antibodies within a day.

A static electrical field causes rapid penetration, since speed scales linearly with the current, but such field also causes damage to the tissue. A stochastic electrical field causes even more rapid penetrtion, since speed scales quadratically with the current, and it has minimal tissue damage and enables more uniform staining. The main challenge in stochastic electrotransport is building the chamber and buffer flow system. The design is publicly available (`www.chunglabresources.com`), but a commercial option is expected soon from LifeCanvas Technologies (`www.lifecanvastech.com`).

Lee et al. (2016) demonstrated a simpler and cheaper active method based on applying pressure to increase the speed and depth of dyes and antibodies penetration into the tissue, coined PRESTO (Pressure-Related Efficient and Stable Transfer of macromolecules into Organs, part of the ACT-PRESTO protocol). Centrifugal force (c-PRESTO) or convection flow (*s*-PRESTO; for *s*yringe) enabled rapid ICH in 100 μm thick sections within 2–3 h, which compared to passive diffusion requires 1-2 days. *c*-PRESTO requires a standard

standard table-top centrifuge, while *s*-PRESTO requires a syringe pump.

RNA studies

Strands of RNA are fixed by PFA and retained in the hydrogel, but the potential histological value from RNA is so far unexplored in most clearing methods. Single-molecule fluorescence in-situ hybridization (smFISH) of RNA has been demonstrated in thin (100 μm) PACT-processed sections (Yang et al., 2014). By adding a polymerisation step, hybridization chain reaction (smHCR), the depth of RNA detection is extended to 500 μm (Shah et al., 2016). Which can visualise e.g. bacterial infections (DePas et al., 2016).
However, a modified protocol, EDC-CLARITY, uses carbodiimide chemistry to fix 5' terminal phosphates to bind and preserve small RNAs and presents several methods of RNA amplification to study RNA in larger tissues (Sylwestrak et al., 2016). It uses a less rigid hydrogel (4% PFA, 1% Acrylamide and 0.00625% Bis-acrylamide) and an EDC (1-Ethyl-3-(3-dimethylaminopropyl)carbodiimide) fixation step before clearing to retain even microRNA. Depending on the length of the oligonucleotide probe, the probe can be amplified by several strategies i.e. Digoxigenin-labeled LNAs and Tyramide Signal Amplification that enables measurement of activity-dependent transcriptional signatures, cell-identity markers, and diverse non-coding RNAs in large tissue volumes (Sylwestrak et al., 2016).

Lipid and membrane stains

Fluorescent dyes, such as the generic *DiI*, *DiD* and other carbocyanine dyes, are lipophilic and therefore primarily stain cellular membranes. They are extensively used for retro- and anterograde neuronal labelling as well as for marking the position of extracellular electrodes after electrophysiology. CLARITY and other clearing techniques, such Sca/e and CUBIC (Hama et al., 2011; Susaki et al., 2014) essentially work by washing away the lipids with detergents and solvents. As an unintended consequence, the clearing process therefore also washes out lipophilic dyes, since they adhere to the lipids (Chung et al., 2013; Richardson and Lichtman, 2015; Tainaka et al., 2016). Yet, there are CLARITY-compatible lipophilic and membrane dyes, which can circumvent this problem. DiI—analogues, sulfonated DiI–variants (SP-DiI), and DiI with a chloromethyl benzamide modification (CM-DiI) are aldehyde-fixable to proteins and reliable remain and fluoresce stable in PACT treated tissue (Jensen and Berg, 2016). An alternative is to stain the membranes post-mortem or after tissue-clearing, even with fixable (SP-DiI) or regular DiI (Jensen and Berg, 2016; Xavier et al., 2017). Similarly, the smaller lipophilic FM dyes, are used to image synaptic vesicle exocytosis and endocytosis and has an analogous chemical structure to DiI. FM 1–43FX is a modified FM dye with an aldehyde–fixable aliphatic amine terminal, that also reliable remains and fluoresces stable in PACT treated tissue (Jensen and Berg, 2016).
Since the DiI–analogues are covalently bound to primary amines on proteins by methylene bridges following aldehyde fixation, they are not removed during lipid extraction by solvents or detergents. Other membrane probes that have a aldehyde-fixable anchor point such as mCLING (Revelo et al., 2014) are likely also CLARITY-compatible. Despite the lipid removal and disruption of the lipid membranes, it is possible to perform immunocytochemistry on membrane associated proteins e.g. tight junctions proteins (e.g. Zonula Occludens-1) and channels (e.g. Aquaporin-4) (Neckel et al., 2016).

Other dyes

Neuronal labelling using the generic amide *biocytin* is an intracellular dye, which is CLARITY-compatible. The delivery of biocytin into the neuronal cytoplasm is usually accomplished either by an intracellular electrode after electrophysiological recording (Petersen et al., 2014; Vestergaard and Berg, 2015; Petersen and Berg, 2016) or by uptake from the nearby surroundings left by juxtacellular deposits in association with extracellular recordings (Wilson and Sachdev, 2004). Biocytin is not washed out of the cell during CLARITY and can be stained with streptavidin conjugated dye (e.g. Cyanine-3) akin to regular ICH (unpublished observations, Jensen and Berg).
CLARITY can also be combined with classical histology such as Hematoxylin-Eosin and Heidenhain's Azan

stain, suggesting potential use in histopathology (Neckel et al., 2016) or combined with colorimetric (non-fluorescent) methods such as horseradish peroxidase conversion of diaminobenzidine to a coloured insoluble product (Sung et al., 2016).

Minimizing autofluorescence

Two primary sources of autofluorescence in CLARITY treated tissue are heme and lipofuscin.
It is therefore important to remove as much blood as possible to reduce the autofluorescent signal from heme. Under normal conditions, blood is removed during the initial cardiac perfusion, but in special situations where perfusion is not possible, such as in human tissue, heme can be eluted by incubating hydrogel-embedded PACT sections in aminoalcohol (CUBIC reagent-1: mixture of 25% (w/v) urea, 25% (w/v) N,N,N',N'-tetrakis(2-hydroxypropyl) ethylenediamine and 15% (w/v) Triton X-100 (Susaki et al., 2014), or 25% (w/v) N,N,N',N'-tetrakis(2-hydroxypropyl) ethylenediamine in PBS alone for 12-24 h at 37°C while shaking before (Treweek et al., 2015) or after clearing (Greenbaum et al., 2017).
Lipofuscin autofluorescence is partially countered by the tissue clearing process. However, when the tissue sections are thick, they may be incubated in 0.2%-1.0% (w/v) Sudan Black B (a nonfluorescent lipophilic dye) in 70% ethanol for 1-3 hours immediately before hydrogel-polymerisation in order to further reduce high autofluorescent background (Treweek et al., 2015).

Table 3: **Different protocols and improvements based on CLARITY**
*In mPACT, the process of incubation with monomer solution and the addition of VA-044 and the polymerisation are separate processes.
†Monomers: A: acrymalide and B: bis-acrymalide

Protocol	**Improvement**	**Monomers†**	**Clearing**	**Staining**	**Reference**
CLARITY	The original	PFA, A ,B	ETC-based or passive clearing	IHC by passive diffusion	Chung and Deisseroth (2013); Tomer et al. (2014)
PACT	Improved passive clearing	A	Passive clearing	IHC/RNA by passive diffusion	Yang et al. (2014); Treweek et al. (2015)
PARS	Perfusion-based clearing	A	Perfusion-based clearing	IHC/RNA by passive diffusion	Yang et al. (2014); Treweek et al. (2015)
ePACT	For expansion microscopy	A, B, sodium acrylate	Passive clearing and collagenase digestion	IHC by passive diffusion	Treweek et al. (2015)
CLARITY-TDE	Improved optical clearing by TDE	PFA, A, B	ETC-based clearing	IHC by passive diffusion	Costantini et al. (2015)
Stochastic Electrotransport	Improved active clearing and staining	PFA, A, B	ETC-based clearing with rotating field	IHC by stochastic electrotransport	Kim et al. (2015)
EDC-CLARITY	RNA retention & amplification	PFA, A, B	EDC-fixation before ETC-based clearing	RNA amplification	Sylwestrak et al. (2016)
mPACT	Improved passive clearing	A*	Passive clearing (PACT) with α-thioglycerol	IHC by passive diffusion	Woo et al. (2016)
ACT	Improved active clearing	A	ETC-based clearing with an electrode plate	–	Lee et al. (2016)
PRESTO	Improved tissue staining	A	–	IHC by centrifugal or convection flow	Lee et al. (2016)
FASTClear	Acrylamid-free CLARITY	*none*	Passive clearing (PACT)	IHC by passive diffusion	Lai et al. (2016); Liu et al. (2016)
Other	**Improvement**		**Clearing**	**Staining**	**Reference**
	Staining with lipophilic dyes	–		Fixable lipophilic (DiI and FM) dyes	Jensen and Berg (2016)
	Faster tissue clearing	–	Elevation of clearing temperature to 42–47°C		Yu et al. (2017); Epp et al. (2015)
Bone CLARITY	Specific for bone tissue	A	Decalcify with 10% EDTA		Greenbaum et al. (2017)
PEA-CLARITY	Specific for plant tissue	PFA, A, B	Enzymatic degradation of cell wall		Palmer et al. (2015)

Table 4: **Imaging solutions.**
The RI of each solution can de adjusted by adjusting the concentration of the main ingredient e.g. Histodenz to the optimal RI of the tissue or microscope objective. Brain tissue usually has an average RI of 1.46–1.47, whereas bone has 1.48–1.49. Prices are approximate.

	FocusClear	**RIMS**	***n*RIMS**	**sRIMS**	**TDE**	**Glycerol**	**PROTOS**
Price/100mL	2,880$	280$	75$	5$	5$	15$	200$
Transparency	+++	+++	+++	++	++	++	+++
Main ingredients	diatrizoic acid	88% (w/v) iohexol	80% (w/v) iomeprol	70% (w/v) sorbitol	63% (v/v) 2,2′-thiodiethanol	80% (v/v) glycerol	23.5% (w/v) *n*-methyl-*d*-glucamine 29.4% (w/v) diatrizoic acid 32.4% (w/v) iodixanol
Detergent	proprietary	0.1% Tween-20	0.1% Tween-20	0.1% Tween-20	0.1% Tween-20	0.1% Tween-20	–
Buffer	proprietary	PBS, pH 7.5	PBS, pH 7.5	PBS, pH 7.5	PBS, pH 7.5	PBS, pH 7.5	H_2O

5. Optical Clearing

The final step before imaging is optical clearing, a process where the average refractive index (RI) of the hydrogel (∼1.46) and the imaging solution are closely matched to homogenise the microscopic environment. Photons from both the excitation light and the emitted fluorescence signal scatter when travelling through the sample due to the inherent inhomogeneous RI of tissues, which limits the quality and depth of imaging. The RI of each solution can de adjusted by adjusting the concentration of the main ingredient (e.g. Histodenz) to the optimal RI of the tissue or microscope objective. Brain tissue usually has an average RI of 1.46-1.47, whereas e.g. bone has 1.48-1.49. It is possible to image without a mounting solution, but in simple water or PBST e.g. PBST (0.1% Triton X- 100 in PBS) (Poguzhelskaya et al., 2014). However, the tissue remains swollen, and water and PBST have a lower RI (∼1.33) than of the hydrogel (∼1.46) and therefore the tissue sample will appear opaque or cloudy. Imaging in water is part of the ePACT method where the tissue is intentionally expanded for greater resolution. There are several different options of mounting solutions (**table 4**).

FocusClear: the generic imaging solution

The original FocusClear (CelExplorer Labs Co.)with the main ingredient diatrizoic acid has an RI of 1.454 similar to the tissue-hydrogel, but is expensive (29 US$/ml), and not usable for storage (Tomer et al., 2014). Also, if the sample is not washed properly in PBST, a *irreversible* white precipitate (likely caused by a reaction with remaining SDS) can develop within the embedded tissue after a few days.

RIMS and *n*RIMS: the optimal solutions

Yang et al. (2014) developed an affordable alternative to FocusClear coined *r*efractive *i*ndex *m*atching *s*olution (RIMS) of 88% (w/v) Histodenz in PBS with an RI of 1.46. Both Diatrizoic acid and Iohexol (HistoDenz) are complex molecules containing an aromatic ring and three iodine atoms, which provides a large number of electrons for interaction with passing light waves (i.e., high refractive index), but in a relatively low-concentration and low-viscosity solution (Richardson and Lichtman, 2015). Woo et al. (2016) used a 80% (w/v) solution of Iomeprol-d3 (also known as Nycodenz and Iohexol-d5), referred to as *n*RIMS, which also has an RI of 1.46. A similar solution is PROTOS (Murray et al., 2015). RIMS reportedly works best for rodent brains and is reportedly less ideal for human brain tissue, where 47% TDE in PB is best (Liu et al., 2015).

Glycerol, Sorbitol and TDE: affordable alternatives

Glycerol, Sorbitol, and Thiodiglycol (2,2'-Thiodiethanol, TDE) are water-soluble and low-viscosity liquids that can be used to tune an aqueous solution over a range of refractive indices by dilution in water. Glycerol and sorbitol are inexpensive and conventional clearing reagents and ingredients in mounting media. TDE was initially used in mounting media for super-resolution microscopy (Staudt et al., 2006), but at concentrations of 40-60% (v/v) can also clear large tissues i.e. rodent brains (Costantini et al., 2015; Aoyagi et al., 2015). 63% (v/v) TDE, 80% (v/v) Glycerol, and 70% (w/v) sorbitol (coined sRIMS) by all have an RI of ∼1.46. One drawback to TDE is that, at high concentrations, it reduces the brightness of some green fluorophores (Staudt et al. (2006) and table 1). 47% TDE in PB (instead of PBS) is reportedly better for RI-matching in human tissues (Liu et al., 2015). RIMS outperformed sRIMS and glycerol regarding imaging resolution and depth (Yang et al., 2014; Marx, 2014). Another option is a mix of DMSO and *D*-sorbitol (Economo et al., 2016).

Storage of CLARITY tissue

All solutions apart from FocusClear can be used for storage. However, a slight loss of fluorescent signal of AlexaFluor-568 has been reported in glycerol (Liu et al., 2015), although the fluorescent signal loss of (red) DiI-dyes has not been observed over 6 months in glycerol (Jensen and Berg, 2016). Storage at

room temperature as opposed to using refrigeration is recommended as precipitate can appear at lower temperatures. All solutions should include 0.01% sodium azide to prevent bacterial growth and an anti-fungal agent for sRIMS. Lowering the PBS concentration to 0.005 M phosphate buffer reduces the appearance of salt precipitate at colder temperatures i.e. 4°C (Treweek et al., 2015).

6. Imaging CLARITY tissue

Imaging of the clarified tissue is more difficult than conventional histological samples. The point of the lipid removal is to make the tissue transparent for the purpose of imaging in depth. This changes the task from imaging single or several 2-dimensional (2D) sections to a 3-dimensional (3D) volume, which is a much larger volume than what is used in conventional microscopy. Such imaging requires considerations of imaging time and resolution when selecting the microscope and objective as well as sample size.

Choice of microscope

Standard light microscopy is generally not suitable for large transparent tissues samples as the excitation light penetrates the sample and generates fluorescence signal from the whole sample. The signal from the focused plane will be attenuated and likely lost by the fluorescence coming from elsewhere. While it is possible to image highly florescent neurons 600 μm deep in 2 mm tissue, the image requires post-processing deconvolution (Epp et al., 2015). However, a low magnification (i.e. 1.5-5×) wide field or stereo microscope can be helpful in an initial and quick examination of tissue for easily identifiable fluorescence signals from e.g. labelled electrode traces before further investigation (Jensen and Berg, 2016; Petersen and Berg, 2016).

Two-photon microscopy, due to only simultaneous absorption of two photons results in fluorescence signal emission leads to lower photobleaching and may also provide greater imaging depths than confocal microscopy, but its serial point–by–point scanning in 3D tissue is similarly slow.

Light-sheet microscopy is a 3D imaging technique is ideal for clarified samples. Light-sheet microscopy achieves optical sectioning by selectively confining the illumination to the plane of interest by using a Gaussian or Bessel beam from the side of the tissue. Furthermore, while confocal and two-photon microscopy is point scanning, and hence inherently slow, light-sheet microscopy uses fast sCMOS or CCD camera sensors to image the selectively illuminated focal plane, resulting in minimal photobleaching and increased imaging speeds that are 2–3 orders of magnitude faster than confocal and two-photon microscopy (Tomer et al., 2014).

Microscope objectives

Objectives with high numerical aperture and long working distances are desirable for maximum imaging depth and resolution. Furthermore, objectives should be optimised for an RI of 1.46 for CLARITY cleared tissues. Several objectives have been developed specifically for CLARITY (**table 5**).
When using a non-optimized objective, it is best to use the one designed for the RI near 1.46 e.g. glycerine (RI 1.47) or oil immersion (RI 1.52). Water-immersion lenses (RI 1.33) work better than air objectives (RI 1). Furthermore, it is time-consuming imaging a large area using a 25× objective, since this requires capturing and stitching of multiple tiles of images. Such strategy also increases the risk of photobleaching. A lower magnification 10x can be more useful to image over larger areas, and they have longer working distances. Indeed, the affordable and commonly available low magnification (10-20×) air lenses are compatible and have been successfully used for several CLARITY studies (Jensen and Berg, 2016; Hsiang et al., 2014; Poguzhelskaya et al., 2014; Bastrup and Larsen, 2017). CLARITY-based tissue clearing provided an increased signal-to-noise ratio, and staining homogeneity in super-resolution stimulated emission depletion (STED) microscopy (i.e. with a 100× objective) of kidney tissue (Unnersjö-Jess et al.).
During hour-long imaging water can evaporate from the imaging medium and subtlety change RI and lead to aberrations and loss of resolution a high imaging depths. A hygroscopic imaging media e.g. with TDE, or imaging in a sealed chamber prevents this.

Table 5: **Microscope objectives optimised for imaging CLARITY samples**

Model	Manufacturer	Numerical Aperture	Magn.	Working Distance	Refractive Index
XLPLN10×SVMP	*Olympus*	0.6	10×	8.0 mm	1.33—1.52
LSFM Clearing 20×/1.0	*Zeiss*	1.0	20×	5.6 mm	1.45
Clr Plan-APOCHROMAT 20×/1.0 Corr	*Zeiss*	1.0	20×	5.6 mm	1.45
Clr Plan-NEOFLUAR 20×/1.0 Corr	*Zeiss*	1.0	20×	5.6 mm	1.45
HC FLUOTAR L 25×/1.00 IMM motCORR VISIR	*Leica*	1.0	25×	6.0 mm	1.46
XLSLPN25×GMP	*Olympus*	1.0	25×	8.0 mm	1.41—1.52

Stereology

Quantification of total cell numbers, densities and projections in tissue while preserving spatial information has been a challenge in *stereology*, since it relies on interpretation of 2D sections of tissues and statistical sampling methods from several histological tissue sections (Gundersen and Jensen, 1987; Walloe et al., 2011). Applying stereological methods to cleared tissues eliminates the need for labour-intensive sectioning. Furthermore, clearing and counting in the whole 3D volumes rather than multiple sampled 2D sections allows for better stereological estimates and also has the advantage of the ability to detect subtle changes that might be overlooked because of sampling variance (Erskine and Khundakar, 2016; Greenbaum et al., 2017; Bastrup and Larsen, 2017). However, the computational challenge of aligning images, down-sampling, and creating a 3D visualisation are currently only semi-automated and for many investigators such task represents a strain. The performance of automated cell detection and segmentation algorithms as alternatives to manual stereological cell counting are still limited by lower detection rates and higher false-positive rates (Schmitz et al., 2014).

Author recommendations

Several qualities are worth considering when selecting or optimising a CLARITY protocol (**figure 3**). From our experience we recommend the following:

For most tissue use PACT or mPACT: The passive protocols are uncomplicated and inexpensive to setup for novel users. The protocols that omits PFA result in faster clearing with less protein loss and better staining. However, we also recommend including 0.05% bis-acrylamide in the monomer solution because it makes for a more rigid hydrogel and the solidification of the monomer solution surrounding the tissue is an indicator of successful polymerisation, although this may also slow the clearing. Clearing speed can further be improved by elevating the temperature during clearing to 42-47°C and employing mPACT. A minimalist incubation chamber can be built using a styrofoam box with a temperature–controlled heating pad, and then placing the box and a gentle lab shaker.

For large tissues use ETC: For active clearing of large tissues with a simple ETC chamber with single wires for thick tissue sections (1-3 mm), we recommend the design by Bastrup and Larsen (2017) where the distance between wires can easily be adjusted and enables tissue clearing of variable tissue sizes while minimising the resistance and limiting the heat generated in the system. For whole brains or organs, we recommend the more elaborate Stochastic Electrotransport approach. The addition of 0.5% α-thioglycerol to prevent tissue discolouration during electrophoresis recommended regardless of chamber design.

Use glycerol and RIMS: Selecting an imaging solution is a decision of price and quality. We regularly use 80% glycerol and RIMS for imaging and storage. See **table 4** for options of mounting solutions.

Figure 3: **Desirable qualities when selecting and optimising a CLARITY-protocol.**

Successful applications using CLARITY

CLARITY is applicable not only to nervous tissue, but in principle to any biological tissue.
The spinal cord is enveloped by dense grey matter, and the myelin can be difficult, although not impossible, to clear, and limits access to the internal white matter (Jensen and Berg, 2016; Spence et al., 2014; Liang et al., 2015, 2016). One simple solution is to split the spinal cord down the midline into two hemisections, which may be easier to stain and image than using PARS-CSF.
While CLARITY was originally demonstrated in mice and rat brains, CLARITY and its variants have been used in several other tissues and organisms.
Zebrafish are a popular neuroscience model organism and can be cleared in PACT (compared to CLARITY), but with an added 5% DMSO to the monomer solution to increase penetration into the tissue and 1% PFA and 0.05-0.025% bis-acrylamide) to increase rigidity of the tissue (Cronan et al., 2015; Frétaud et al., 2017).

Human samples

Human brain samples from clinical biobanks open the possibility of visualising human pathology, but clinical samples are usually fixated in formalin and may have been stored for a prolonged period. Indeed, the human pathology of Alzheimer's (Ando et al., 2014), Parkinson's (Liu et al., 2015), neurodegeneration due to

mitochondrial disease (Phillips et al., 2016) and neurodevelopmental disorders i.e. autism (Chung et al., 2013) and drug-resistant epilepsy due to hemimegaloencephaly (Costantini et al., 2015) have been visualised in 3D by CLARITY on formalin-fixed tissues. One frozen brain sample (PFA-fixed and cryoprotected in sucrose) has also been cleared and stained using CLARITY (Phillips et al., 2016), and the human enteric nervous system as well (Neckel et al., 2016). The speed of tissue clearing differs between CNS regions depending on the degree of myelination and the duration of formalin fixation.
The transient tissue expansion during CLARITY-clearing of animal tissue has been observed in human brain tissues, especially after prolonged (>40 days) passive tissue clearing, to be irreversible (Liu et al., 2015). Lai et al. (2016) demonstrated an acrylamide-free version of CLARITY, i.e. essentially only washing with SDS followed by RIMS, which gave better results for formalin-fixed tissue, while also arguing that the tissue-PFA-acrylamide cross-linking is only theoretical and does not actually occur. For this reason, omitting acrylamide is easier and better, which they have developed into a protocol named Free of acrylamide sodium dodecyl sulphate (SDS)-based tissue-clearing (FASTClear) protocol (Liu et al., 2016).

Beyond the CNS

The enteric nervous system and mesenteric vasculature can be visualised in 3D with CLARITY (Neckel et al., 2016). While it is possible to clear skeletal muscle with CLARITY, labelling the neuromuscular junctions with fluorescently labelled α-bungarotoxin has not been possible, likely due to the cross-linking and fixation preventing the access of the toxin to the acetylcholine receptors (Milgroom and Ralston, 2016). However peripheral nerves could be targeted by ICH or an anterograde lipophilic tracer e.g. SP-DiI or a viral tracer instead. It remains to be tested whether labelling of Isolectin B4-positive nociceptor cells is compatible with CLARITY clearing. Neurovasculature has also been studied, where the tissue is incubated in or the vasculature is flushed with antibodies for blood vessel endothelial cells, i.e. anti-CD31 (Neckel et al., 2016; Woo et al., 2016), but could also be stained by flushing the vasculature with a DiI-dye or biocytin before fixation.

Muscle and bone

It is possible to clear skeletal, cardiac and smooth muscle with CLARITY-based clearing with no modifications to the protocols (Yang et al., 2014; Epp et al., 2015; Milgroom and Ralston, 2016; Gloschat et al., 2016; Kolesová et al., 2016; Sung et al., 2016). However, the collagen-rich tendons, similar to the myelin-rich white mater of the spinal cord, are difficult to make transparent. They have not specifically been the focus of a study, but extended clearing time and adjustment of the RIMS RI may improve tendon transparency. If desired the chondrocytes can be stained with the fixable lipophilic dye, DiI-SP (Jensen and Berg, 2016; Calve et al., 2015).
Bone tissue, however, poses a problem given that it has a solid, hard mineral component in addition to the soft bone marrow. Clearing osseous tissue is usually done by a solvent based methods (Richardson and Lichtman, 2015; Greenbaum et al., 2017). Bone can be cleared with CLARITY by adding a decalcification step, PACT-deCAL, in which tissue is placed in a 0.1 M EDTA (in PBS, pH 8 for 2 days) intermediately during PACT-clearing with increased SDS concentration and pH (8-10% SDS and pH 8), however, this gave only modest visualisation depth of 200-300 μm (Treweek et al., 2015).
By extending and increasing the decalcification step (0.3 M EDTA and 14 days) Gradinaru's group was able to extend visualisation depth to 1.5 mm in a protocol called 'Bone CLARITY' (Greenbaum et al., 2017). The heme-rich bone marrow also presents a problem regarding autofluorescence, which was be reduced by removing heme with amino alcohol before refractive index matching (**figure 4**). The osteoblasts can be stained with the fixable lipophilic dye CM-DiI (Jensen and Berg, 2016; van Gastel et al., 2012).

Other organs and species

CLARITY-based protocols have been used with little (e.g. lower acrylamide concentrations) or no modifications to clear most other organs such as lever (Lee et al., 2014; Font-Burgada et al., 2015), kidney (Yang

PACT	Fixation			Hydrogel Polymersiation	Lipid Removal			Wash			Refactive Index Matching
Treweek et al. 2016	Transcardial PFA-fixation			As in PACT (A4P0)	As in PACT (8% SDS, pH 7.5, 37°C) 4 - 5 days			In PBS x 3 over 1 day			Incubation in RIMS RI 1.47 overnight

PACT deCAL	Fixation			Hydrogel Polymersiation	Lipid Removal	Decalification	Lipid Removal	Wash			Refactive Index Matching
Treweek et al. 2016	Transcardial PFA-fixation			As in PACT (A4P0)	8-10% SDS, pH 8, at 37°C for 24 hrs	3% w/v (0.1 M) EDTA in PBS, pH 8, at 37°C for 2 days	8-10% SDS, pH 8, at 37°C for 24 hrs	In PBS x 3 over 1 day			Incubation in RIMS RI 1.48-1.49 overnight

Bone CLARITY	Fixation	Post-Fixation	Decalification	Hydrogel Polymersiation	Lipid Removal			Wash	Heme auto-fluorescence removal	Wash	Refactive Index Matching
Greenbaum et al. 2017	Transcardial PFA-fixation	Extracted tissue post-fixed overnight in PFA	10% w/v (0.34 M) EDTA in PBS, pH 8, with stirring at 4°C and daily buffer exchange for 2 weeks	As in PACT (A4P0)	As in PACT (8% SDS, pH 7.5, at 37°C) 4 - 5 days			In PBS x 3 over 2 days	25% w/v amino alcohol in PBS, pH 9, at 37C with stirring	In PBS x 3 over 2 days	Stepwise incubation over 3 days in RIMS RI 1.38, 1.43, 1.47

Figure 4: **CLARITY protocols for bone tissue clearing**
It is possible to clear bone tissue by decalcification with EDTA (ethylenediaminetetraacetic acid) prior or intermediate during lipid removal. The PACT deCAL protocol only allows for a limited visualisation depth of <0.2mm, whereas the Bone CLARITY protocol allows up to 1.5mm. The amino alcohol is N,N,N',N'-tetrakis(2-hydroxypropyl)ethylenediamine is used to remove heme from the bone marrow. ICH is as usual done before RI-matching. Osteoblasts are stainable with the fixable lipophilic dye CM-DiI (Jensen and Berg, 2016; van Gastel et al., 2012). Cleared bone should be incubated in RIMS with RI 1.48-1.49 (Treweek et al., 2015), but RI 1.47 is recommended when imaging the bone and marrow simultaneously (Greenbaum et al., 2017).

et al., 2014; Lee et al., 2014; Unnersjö-Jess et al.), pancreas (Lee et al., 2014; Muzumdar et al., 2016), adrenal gland (Epp et al., 2015), spleen (Epp et al., 2015; Kieffer et al., 2017), lymphoid tissues (Kieffer et al., 2017), intestine (Yang et al., 2014; Lee et al., 2014; Epp et al., 2015; Neckel et al., 2016; Kieffer et al., 2017), testes (Epp et al., 2015; Frétaud et al., 2017), ovaries (Feng et al., 2017), and lung tissue (Yang et al., 2014; Lee et al., 2014; Epp et al., 2015; Saboor et al., 2016).
However, given that organs have different densities and ratios of connective tissue, lipids, and protein the clearing times vary (**table 2**), and the average RI of the tissue-hydrogel does as well. For spleen and kidney, the best RI-matching solutions were found to be CUBIC-mount, RIMS, sRIMS and TDE, respectively (Lee et al., 2016).
Vertebrate and invertebrate model animals, such as rabbits, chickens, zebrafish, xenopus, small octopuses were cleared by the ACT (Lee et al., 2016). Other models include sea lamprey (Chung-Davidson et al., 2014) and pond turtles (unpublished observations, Jensen and Berg).
Adding an enzymatic degradation step as in Plant-Enzyme-Assisted (PEA)-CLARITY, it is possible to remove the plant cell walls after tissue-clearing in SDS (which inhibits the enzymes) to clear and stain whole plant tissues without the need for any sectioning of the material, thus facilitating molecular phenotyping and protein localisation of intact tissue in 3D, whilst retaining cellular structure (Palmer et al., 2015). CLARITY has also been used with hybridization chain reaction to detect rRNA from and visualise bacterial infections (DePas et al., 2016).

Current limitations and future improvements

Much work has increased the clearing speed of the method CLARITY and adapted its use to several tissue types i.e. non-nervous tissue, bones, and plants. This increases our understanding of various biological events in different organs and species. While ICH in large volumes continues to be difficult, the main limitation seems to be in imaging and data processing of the large volumes. Light-sheet microscopy makes image acquisition fast and easy but is not readily available to all researchers. Furthermore, large image volumes give large data volumes (Giga- to Terabyte) that are difficult to handle and analyse. The challenge of image acquisition and analysis, therefore, lies beyond CLARITY and is a problem shared by all tissue clearing methods. Improvements in large volume image data analysis will improve not only help experimenters using CLARITY, but bring histology into the 3*rd* dimension.

Acknowledgements

We thank Editor-in-chief Dr H. Steinbusch for the invitation for this review. Supported by the Danish Council for Independent Research medical science (R.W.B). The work is part of the Dynamical Systems Interdisciplinary Network, University of Copenhagen.

Conflicts of interest

None

References

K Ando, Q Laborde, A Lazar, D Godefroy, I Youssef, M Amar, A Pooler, MC Potier, B Delatour, and C Duyckaerts. Inside Alzheimer brain with CLARITY: senile plaques, neurofibrillary tangles and axons in 3-D. *Acta Neuropathol*, 128:457–9, Sep 2014.

Y Aoyagi, R Kawakami, H Osanai, T Hibi, and T Nemoto. A rapid optical clearing protocol using 2,2'-thiodiethanol for microscopic observation of fixed mouse brain. *PLoS One*, 10:e0116280, 2015.

Joakim Bastrup and Peter H. Larsen. Optimized CLARITY technique detects reduced parvalbumin density in a genetic model of schizophrenia. *Journal of Neuroscience Methods*, 283:23–32, may 2017. doi: 10.1016/j.jneumeth.2017.03.011. URL https://doi.org/10.1016%2Fj.jneumeth.2017.03.011.

Dawen Cai, Kimberly B Cohen, Tuanlian Luo, Jeff W Lichtman, and Joshua R Sanes. Improved tools for the brainbow toolbox. *Nat. Methods*, 10(6):540–7, 2013. ISSN 1548-7091. doi: 10.1038/nmeth.2450.

Sarah Calve, Andrew Ready, Christopher Huppenbauer, Russell Main, and Corey P. Neu. Optical clearing in dense connective tissues to visualize cellular connectivity in situ. *PLOS ONE*, 10(1):1–14, 01 2015. doi: 10.1371/journal.pone.0116662. URL https://doi.org/10.1371/journal.pone.0116662.

K Chung and K Deisseroth. CLARITY for mapping the nervous system. *Nat Methods*, 10:508–13, Jun 2013.

K Chung, J Wallace, SY Kim, S Kalyanasundaram, AS Andalman, TJ Davidson, JJ Mirzabekov, KA Zalocusky, J Mattis, AK Denisin, S Pak, H Bernstein, C Ramakrishnan, L Grosenick, V Gradinaru, and K Deisseroth. Structural and molecular interrogation of intact biological systems. *Nature*, 497:332–7, May 2013.

Yu-Wen Chung-Davidson, Peter J. Davidson, Anne M. Scott, Erin J. Walaszczyk, Cory O. Brant, Tyler Buchinger, Nicholas S. Johnson, and Weiming Li. A new clarification method to visualize biliary degeneration during liver metamorphosis in sea lamprey (petromyzon marinus). (88):e51648, 2014. ISSN 1940-087X. doi: doi:10.3791/51648. URL https://www.jove.com/video/51648.

I Costantini, JP Ghobril, Giovanna AP Di, Mascaro AL Allegra, L Silvestri, MC Müllenbroich, L Onofri, V Conti, F Vanzi, L Sacconi, R Guerrini, H Markram, G Iannello, and FS Pavone. A versatile clearing agent for multi-modal brain imaging. *Sci Rep*, 5:9808, May 2015.

Mark R. Cronan, Allison F. Rosenberg, Stefan H. Oehlers, Joseph W. Saelens, Dana M. Sisk, Kristen L. Jurcic Smith, Sunhee Lee, and David M. Tobin. Clarity and pact-based imaging of adult zebrafish and mouse for whole-animal analysis of infections. *Disease Models & Mechanisms*, 8(12):1643–1650, 2015. ISSN 1754-8403. doi: 10.1242/dmm.021394. URL http://dmm.biologists.org/content/8/12/1643.

William H. DePas, Ruth Starwalt-Lee, Lindsey Van Sambeek, Sripriya Ravindra Kumar, Viviana Gradinaru, and Dianne K. Newman. Exposing the three-dimensional biogeography and metabolic states of pathogens in cystic fibrosis sputum via hydrogel embedding, clearing, and rrna labeling. *mBio*, 7(5), 2016. doi: 10.1128/mBio.00796-16. URL http://mbio.asm.org/content/7/5/e00796-16.abstract.

Michael N Economo, Nathan G Clack, Luke D Lavis, Charles R Gerfen, Karel Svoboda, Eugene W Myers, and Jayaram Chandrashekar. A platform for brain-wide imaging and reconstruction of individual neurons. *eLife*, 5:e10566, jan 2016. ISSN 2050-084X. doi: 10.7554/eLife.10566. URL https://dx.doi.org/10.7554/eLife.10566.

Jonathan R. Epp, Yosuke Niibori, Hwa-Lin (Liz) Hsiang, Valentina Mercaldo, Karl Deisseroth, Sheena A. Josselyn, and Paul W. Frankland. Optimization of clarity for clearing whole-brain and other intact organs. *eNeuro*, 2(3), 2015. doi: 10.1523/ENEURO.0022-15.2015. URL http://eneuro.org/content/2/3/ENEURO.0022-15.2015.

D. Erskine and A.A. Khundakar. Stereological approaches to dementia research using human brain tissue. *Journal of Chemical Neuroanatomy*, 76, Part B:73 – 81, 2016. ISSN 0891-0618. doi: https:

//doi.org/10.1016/j.jchemneu.2016.01.004. URL http://www.sciencedirect.com/science/article/pii/S0891061816000065. Unbiased Stereology of Neural Systems: From Normal Aging to Mental Illness and Neurodegenerative Diseases.

Yi Feng, Peng Cui, Xiaowei Lu, Brian Hsueh, Fredrik Möller Billig, Livia Zarnescu Yanez, Raju Tomer, Derek Boerboom, Peter Carmeliet, Karl Deisseroth, and Aaron J. W. Hsueh. Clarity reveals dynamics of ovarian follicular architecture and vasculature in three-dimensions. *Scientific Reports*, 7:44810, 2017. doi: 10.1038/srep44810https://www.nature.com/articles/srep44810#supplementary-information. URL http://dx.doi.org/10.1038/srep44810.

Joan Font-Burgada, Shabnam Shalapour, Suvasini Ramaswamy, Brian Hsueh, David Rossell, Atsushi Umemura, Koji Taniguchi, Hayato Nakagawa, Mark?A Valasek, Li Ye, Janel?L Kopp, Maike Sander, Hannah Carter, Karl Deisseroth, Inder?M Verma, and Michael Karin. Hybrid periportal hepatocytes regenerate the injured liver without giving rise to cancer. *Cell*, 162(4):766–779, August 2015. ISSN 0092-8674. doi: 10.1016/j.cell.2015.07.026. URL http://dx.doi.org/10.1016/j.cell.2015.07.026.

Maxence Frétaud, Laurie Rivière, Élodie De Job, Stéphanie Gay, Jean-Jacques Lareyre, Jean-Stéphane Joly, Pierre Affaticati, and Violette Thermes. High-resolution 3d imaging of whole organ after clearing: taking a new look at the zebrafish testis. *Sci Rep*, 7:43012, Feb 2017. ISSN 2045-2322. doi: 10.1038/srep43012. URL http://www.ncbi.nlm.nih.gov/pmc/articles/PMC5314416/. 28211501[pmid].

C. R. Gloschat, A. C. Koppel, K. K. Aras, J. A. Brennan, K. M. Holzem, and I. R. Efimov. Arrhythmogenic and metabolic remodelling of failing human heart. *The Journal of Physiology*, 594(14):3963–3980, 2016. ISSN 1469-7793. doi: 10.1113/JP271992. URL http://dx.doi.org/10.1113/JP271992.

Alon Greenbaum, Ken Y. Chan, Tatyana Dobreva, David Brown, Deepak H. Balani, Rogely Boyce, Henry M. Kronenberg, Helen J. McBride, and Viviana Gradinaru. Bone clarity: Clearing, imaging, and computational analysis of osteoprogenitors within intact bone marrow. *Science Translational Medicine*, 9(387), 2017. ISSN 1946-6234. doi: 10.1126/scitranslmed.aah6518. URL http://stm.sciencemag.org/content/9/387/eaah6518.

H. J G Gundersen and E. B. Jensen. The efficiency of systematic sampling in stereology and its prediction. *Journal of Microscopy*, 147(3):229–263, 1987. ISSN 13652818. doi: 10.1111/j.1365-2818.1987.tb02837.x.

Hiroshi Hama, Hiroshi Kurokawa, Hiroyuki Kawano, Ryoko Ando, Tomomi Shimogori, Hisayori Noda, Kiyoko Fukami, Asako Sakaue-Sawano, and Atsushi Miyawaki. Scale: a chemical approach for fluorescence imaging and reconstruction of transparent mouse brain. *Nat Neurosci*, 14(11):1481–1488, Nov 2011. ISSN 1097-6256. doi: 10.1038/nn.2928. URL http://dx.doi.org/10.1038/nn.2928.

Hwa-Lin Hsiang, Jonathan R Epp, Michel C van den Oever, Chen Yan, Asim J Rashid, Nathan Insel, Li Ye, Yosuke Niibori, Karl Deisseroth, Paul W Frankland, and Sheena A Josselyn. Manipulating a "cocaine engram" in mice. *The Journal of Neuroscience*, 34(42):14115–14127, 2014. ISSN 0270-6474. doi: 10.1523/jneurosci.3327-14.2014. URL http://dx.doi.org/10.1523/jneurosci.3327-14.2014.

KH Jensen and RW Berg. CLARITY-compatible lipophilic dyes for electrode marking and neuronal tracing. *Sci Rep*, 6:32674, Sep 2016.

MT Ke, S Fujimoto, and T Imai. SeeDB: a simple and morphology-preserving optical clearing agent for neuronal circuit reconstruction. *Nat Neurosci*, 16:1154–61, Aug 2013.

Collin Kieffer, Mark S Ladinsky, Allen Ninh, Rachel P Galimidi, and Pamela J Bjorkman. Longitudinal imaging of hiv-1 spread in humanized mice with parallel 3d immunofluorescence and electron tomography. *eLife*, 6:e23282, feb 2017. ISSN 2050-084X. doi: 10.7554/eLife.23282. URL https://dx.doi.org/10.7554/eLife.23282.

Sung-Yon Kim, Jae Cho, Evan Murray, Naveed Bakh, Heejin Choi, Kimberly Ohn, Luzdary Ruelas, Austin Hubbert, Meg McCue, Sara L Vassallo, Philipp J Keller, and Kwanghun Chung. Stochastic electrotrans-

port selectively enhances the transport of highly electromobile molecules. *Proceedings of the National Academy of Sciences*, 112(46):E6274–E6283, 2015. ISSN 0027-8424. doi: 10.1073/pnas.1510133112. URL http://dx.doi.org/10.1073/pnas.1510133112.

Hana Kolesová, Martin Čapek, Barbora Radochová, Jiří Janáček, and David Sedmera. Comparison of different tissue clearing methods and 3d imaging techniques for visualization of gfp-expressing mouse embryos and embryonic hearts. *Histochemistry and Cell Biology*, 146(2):141–152, 2016. ISSN 1432-119X. doi: 10.1007/s00418-016-1441-8. URL http://dx.doi.org/10.1007/s00418-016-1441-8.

Hei Ming Lai, Alan King Lun Liu, Wai-Lung Ng, John DeFelice, Wing Sang Lee, Heng Li, Wen Li, Ho Man Ng, Raymond Chuen-Chung Chang, Bin Lin, Wutian Wu, and Steve M. Gentleman. Rationalisation and Validation of an Acrylamide-Free Procedure in Three-Dimensional Histological Imaging. *PLOS ONE*, 11 (6):e0158628, jun 2016. doi: 10.1371/journal.pone.0158628. URL https://doi.org/10.1371%2Fjournal.pone.0158628.

Eunsoo Lee, Jungyoon Choi, Youhwa Jo, Joo Yeon Kim, Yu Jin Jang, Hye Myeong Lee, So Yeun Kim, Ho-Jae Lee, Keunchang Cho, Neoncheol Jung, Eun Mi Hur, Sung Jin Jeong, Cheil Moon, Youngshik Choe, Im Joo Rhyu, Hyun Kim, and Woong Sun. Act-presto: Rapid and consistent tissue clearing and labeling method for 3-dimensional (3d) imaging. *Scientific Reports*, 6:18631, 2016. ISSN 2045-2322. doi: 10.1038/srep18631. URL http://dx.doi.org/10.1038/srep18631.

H Lee, JH Park, I Seo, SH Park, and S Kim. Improved application of the electrophoretic tissue clearing technology, CLARITY, to intact solid organs including brain, pancreas, liver, kidney, lung, and intestine. *BMC Dev Biol*, 14:48, Dec 2014.

Jun Li, Daniel M Czajkowsky, Xiaowei Li, and Zhifeng Shao. Fast immuno-labeling by electrophoretically driven infiltration for intact tissue imaging. 5:10640, 2015. doi: 10.1038/srep10640. URL http://dx.doi.org/10.1038/srep10640.

Huazheng Liang, Shaoshi Wang, Richard Francis, Renee Whan, Charles Watson, and George Paxinos. Distribution of raphespinal fibers in the mouse spinal cord. *Molecular Pain*, 11:s12990–015–0046–x, 2015. doi: 10.1186/s12990-015-0046-x. URL http://dx.doi.org/10.1186/s12990-015-0046-x.

Huazheng Liang, Emma Schofield, and George Paxinos. Imaging serotonergic fibers in the mouse spinal cord using the clarity/cubic technique. (108):e53673, 2016. ISSN 1940-087X. doi: doi:10.3791/53673. URL https://www.jove.com/video/53673.

Alan K Liu, Madeleine E Hurry, Olivia T Ng, John DeFelice, Hei M Lai, Ronald K Pearce, Gordon T Wong, Raymond C Chang, and Steve M Gentleman. Bringing clarity to the human brain: visualisation of lewy pathology in three-dimensions. *Neuropathology and applied neurobiology*, 2015. ISSN 1365-2990. doi: 10.1111/nan.12293. URL http://dx.doi.org/10.1111/nan.12293.

Alan King Lun Liu, Hei Ming Lai, Raymond Chuen-Chung Chang, and Steve M Gentleman. Free-of-acrylamide sds-based tissue clearing (fastclear): A novel protocol of tissue clearing for three-dimensional visualisation of human brain tissues. *Neuropathology and Applied Neurobiology*, 2016. ISSN 1365-2990. doi: 10.1111/nan.12361. URL http://dx.doi.org/10.1111/nan.12361.

Chiara Magliaro, Alejandro L. Callara, Giorgio Mattei, Marco Morcinelli, Cristina Viaggi, Francesca Vaglini, and Arti Ahluwalia. Clarifying CLARITY: Quantitative Optimization of the Diffusion Based Delipidation Protocol for Genetically Labeled Tissue. *Frontiers in Neuroscience*, 10, apr 2016. doi: 10.3389/fnins.2016.00179. URL https://doi.org/10.3389%2Ffnins.2016.00179.

Vivien Marx. Microscopy: seeing through tissue. *Nature Methods*, 11(12):1209–1214, nov 2014. doi: 10.1038/nmeth.3181. URL https://doi.org/10.1038%2Fnmeth.3181.

Andrew Milgroom and Evelyn Ralston. Clearing skeletal muscle with clarity for light microscopy imaging.

Cell Biology International, 40(4):478–483, 2016. ISSN 1095-8355. doi: 10.1002/cbin.10578. URL http://dx.doi.org/10.1002/cbin.10578.

Evan Murray, Jae Hun Cho, Daniel Goodwin, Taeyun Ku, Justin Swaney, Sung-Yon Kim, Heejin Choi, Young-Gyun Park, Jeong-Yoon Park, Austin Hubbert, Margaret McCue, Sara Vassallo, Naveed Bakh, Matthew P Frosch, Van J Wedeen, H. Sebastian Seung, and Kwanghun Chung. Simple, scalable proteomic imaging for high-dimensional profiling of intact systems. *Cell*, 163(6):1500–1514, December 2015. ISSN 0092-8674. doi: 10.1016/j.cell.2015.11.025. URL http://dx.doi.org/10.1016/j.cell.2015.11.025.

Mandar Deepak Muzumdar, Kimberly Judith Dorans, Katherine Minjee Chung, Rebecca Robbins, Tuomas Tammela, Vasilena Gocheva, Carman Man-Chung Li, and Tyler Jacks. Clonal dynamics following p53 loss of heterozygosity in kras-driven cancers. *Nature Communications*, 7:12685, 2016. doi: 10.1038/ncomms12685https://www.nature.com/articles/ncomms12685#supplementary-information. URL http://dx.doi.org/10.1038/ncomms12685.

Peter H. Neckel, Ulrich Mattheus, Bernhard Hirt, Lothar Just, and Andreas F. Mack. Large-scale tissue clearing (PACT): Technical evaluation and new perspectives in immunofluorescence histology, and ultrastructure. *Scientific Reports*, 6(1), sep 2016. doi: 10.1038/srep34331. URL https://doi.org/10.1038%2Fsrep34331.

William M. Palmer, Antony P. Martin, Jamie R. Flynn, Stephanie L. Reed, Rosemary G. White, Robert T. Furbank, and Christopher P. L. Grof. Pea-clarity: 3d molecular imaging of whole plant organs. *Scientific Reports*, 5:13492, 2015. doi: 10.1038/srep13492https://www.nature.com/articles/srep13492#supplementary-information. URL http://dx.doi.org/10.1038/srep13492.

Peter C. Petersen and Rune W. Berg. Lognormal firing rate distribution reveals prominent fluctuation-driven regime in spinal motor networks. *eLife*, 5:e18805, 2016. doi: 10.7554/eLife.18805. URL https://elifesciences.org/content/5/e18805.

Peter C. Petersen, Mikkel Vestergaard, Kristian H. R. Jensen, and Rune W. Berg. Premotor spinal network with balanced excitation and inhibition during motor patterns has high resilience to structural division. *Journal of Neuroscience*, 34(8):2774–2784, 2014. ISSN 0270-6474. doi: 10.1523/JNEUROSCI.3349-13.2014. URL http://www.jneurosci.org/content/34/8/2774.

Jonathan Phillips, Alex Laude, Robert Lightowlers, Chris M Morris, Doug M Turnbull, and Nichola Z Lax. Development of passive clarity and immunofluorescent labelling of multiple proteins in human cerebellum: understanding mechanisms of neurodegeneration in mitochondrial disease. *Scientific reports*, 6:26013, 2016. ISSN 2045-2322. doi: 10.1038/srep26013. URL http://dx.doi.org/10.1038/srep26013.

E Poguzhelskaya, D Artamonov, A Bolshakova, O Vlasova, and I Bezprozvanny. Simplified method to perform CLARITY imaging. *Mol Neurodegener*, 9:19, May 2014.

Natalia H. Revelo, Dirk Kamin, Sven Truckenbrodt, Aaron B. Wong, Kirsten Reuter-Jessen, Ellen Reisinger, Tobias Moser, and Silvio O. Rizzoli. A new probe for super-resolution imaging of membranes elucidates trafficking pathways. *The Journal of Cell Biology*, 205(4):591–606, 2014. ISSN 0021-9525. doi: 10.1083/jcb.201402066. URL http://jcb.rupress.org/content/205/4/591.

DS Richardson and JW Lichtman. Clarifying Tissue Clearing. *Cell*, 162:246–57, Jul 2015.

Farhan Saboor, Ansgar N. Reckmann, Claudia U.M. Tomczyk, Dorothea M. Peters, Norbert Weissmann, Andre Kaschtanow, Ralph T. Schermuly, Tatyana V. Michurina, Grigori Enikolopov, Dieter Müller, Andrea Mietens, and Ralf Middendorff. Nestin-expressing vascular wall cells drive development of pulmonary hypertension. *European Respiratory Journal*, 47(3):876–888, 2016. ISSN 0903-1936. doi: 10.1183/13993003.00574-2015. URL http://erj.ersjournals.com/content/47/3/876.

Christoph Schmitz, Brian S. Eastwood, Susan J. Tappan, Jack R. Glaser, Daniel A. Peterson, and Patrick R. Hof. Current automated 3d cell detection methods are not a suitable replacement for manual stereologic

cell counting. *Frontiers in Neuroanatomy*, 8:27, 2014. ISSN 1662-5129. doi: 10.3389/fnana.2014.00027. URL http://journal.frontiersin.org/article/10.3389/fnana.2014.00027.

Sheel Shah, Eric Lubeck, Maayan Schwarzkopf, Ting-Fang He, Alon Greenbaum, Chang Sohn, Antti Lignell, Harry MT Choi, Viviana Gradinaru, Niles A Pierce, and Long Cai. Single-molecule rna detection at depth by hybridization chain reaction and tissue hydrogel embedding and clearing. *Development*, 143(15):2862–2867, 2016. ISSN 0950-1991. doi: 10.1242/dev.138560. URL http://dx.doi.org/10.1242/dev.138560.

Rory D Spence, Florian Kurth, Noriko Itoh, Chandler R Mongerson, Shannon H Wailes, Mavis S Peng, and Allan J MacKenzie-Graham. Bringing clarity to gray matter atrophy. *NeuroImage*, 101:625–32, 2014. ISSN 1053-8119. doi: 10.1016/j.neuroimage.2014.07.017. URL http://dx.doi.org/10.1016/j.neuroimage.2014.07.017.

Thorsten Staudt, Marion C. Lang, Rebecca Medda, Johann Engelhardt, and Stefan W. Hell. 2,2′-Thiodiethanol: A new water soluble mounting medium for high resolution optical microscopy. *Microscopy Research and Technique*, 70(1):1–9, 2006. doi: 10.1002/jemt.20396. URL https://doi.org/10.1002%2Fjemt.20396.

Marzena Stefaniuk, Emilio J. Gualda, Monika Pawlowska, Diana Legutko, Paweł Matryba, Paulina Koza, Witold Konopka, Dorota Owczarek, Marcin Wawrzyniak, Pablo Loza-Alvarez, and Leszek Kaczmarek. Light-sheet microscopy imaging of a whole cleared rat brain with Thy1-GFP transgene. *Scientific reports*, 6:28209, 2016. ISSN 2045-2322. doi: 10.1038/srep28209.

Matthew S. Sulkin, Emily Widder, Connie Shao, Katherine M. Holzem, Christopher Gloschat, Sarah R. Gutbrod, and Igor R. Efimov. Three-dimensional printing physiology laboratory technology. *American Journal of Physiology - Heart and Circulatory Physiology*, 305(11):H1569–H1573, 2013. ISSN 0363-6135. doi: 10.1152/ajpheart.00599.2013. URL http://ajpheart.physiology.org/content/305/11/H1569.

Kevin Sung, Yichen Ding, Jianguo Ma, Harrison Chen, Vincent Huang, Michelle Cheng, Cindy F. Yang, Jocelyn T. Kim, Daniel Eguchi, Dino Di Carlo, Tzung K. Hsiai, Atsushi Nakano, and Rajan P. Kulkarni. Simplified three-dimensional tissue clearing and incorporation of colorimetric phenotyping. *Scientific Reports*, 6(1), aug 2016. doi: 10.1038/srep30736. URL https://doi.org/10.1038%2Fsrep30736.

Etsuo A. Susaki, Kazuki Tainaka, Dimitri Perrin, Fumiaki Kishino, Takehiro Tawara, Tomonobu M. Watanabe, Chihiro Yokoyama, Hirotaka Onoe, Megumi Eguchi, Shun Yamaguchi, Takaya Abe, Hiroshi Kiyonari, Yoshihiro Shimizu, Atsushi Miyawaki, Hideo Yokota, and Hiroki R. Ueda. Whole-brain imaging with single-cell resolution using chemical cocktails and computational analysis. *Cell*, April, publisher=Elsevier, volume=157, number=3, pages=726-739, issn=0092-8674, doi=10.1016/j.cell.2014.03.042, url=http://dx.doi.org/10.1016/j.cell.2014.03.042 2014.

EmilyLauren Sylwestrak, Priyamvada Rajasethupathy, MatthewArnot Wright, Anna Jaffe, and Karl Deisseroth. Multiplexed intact-tissue transcriptional analysis at cellular resolution. *Cell*, 164(4):792–804, 2 2016. ISSN 0092-8674. doi: 10.1016/j.cell.2016.01.038. URL http:https://dx.doi.org/10.1016/j.cell.2016.01.038.

Kazuki Tainaka, Akihiro Kuno, Shimpei I. Kubota, Tatzya Murakami, and Hiroki R. Ueda. Chemical principles in tissue clearing and staining protocols for whole-body cell profiling. *Annual Review of Cell and Developmental Biology*, 32(1):713–741, 2016. doi: 10.1146/annurev-cellbio-111315-125001. URL http://dx.doi.org/10.1146/annurev-cellbio-111315-125001. PMID: 27298088.

R Tomer, L Ye, B Hsueh, and K Deisseroth. Advanced CLARITY for rapid and high-resolution imaging of intact tissues. *Nat Protoc*, 9:1682–97, Jul 2014.

Jennifer B Treweek, Ken Y Chan, Nicholas C Flytzanis, Bin Yang, Benjamin E Deverman, Alon Greenbaum, Antti Lignell, Cheng Xiao, Long Cai, Mark S Ladinsky, Pamela J Bjorkman, Charless C Fowlkes, and Viviana Gradinaru. Whole-body tissue stabilization and selective extractions via tissue-hydrogel hybrids

for high-resolution intact circuit mapping and phenotyping. *Nature protocols*, 10(11):1860–96, 2015. ISSN 1754-2189. doi: 10.1038/nprot.2015.122. URL http://dx.doi.org/10.1038/nprot.2015.122.

David Unnersjö-Jess, Lena Scott, Hans Blom, and Hjalmar Brismar. Super-resolution stimulated emission depletion imaging of slit diaphragm proteins in optically cleared kidney tissue. *Kidney International*, 89(1): 243–247. ISSN 0085-2538. doi: 10.1038/ki.2015.308. URL http://dx.doi.org/10.1038/ki.2015.308.

Nick van Gastel, Sophie Torrekens, Scott J. Roberts, Karen Moermans, Jan Schrooten, Peter Carmeliet, Aernout Luttun, Frank P. Luyten, and Geert Carmeliet. Engineering vascularized bone: Osteogenic and proangiogenic potential of murine periosteal cells. *STEM CELLS*, 30(11):2460–2471, 2012. ISSN 1549-4918. doi: 10.1002/stem.1210. URL http://dx.doi.org/10.1002/stem.1210.

M. Vestergaard and R. W. Berg. Divisive Gain Modulation of Motoneurons by Inhibition Optimizes Muscular Control. *J Neurosci*, 35(8):3711–3723, 2015. ISSN 0270-6474. doi: 10.1523/JNEUROSCI.3899-14.2015. URL http://www.jneurosci.org/cgi/doi/10.1523/JNEUROSCI.3899-14.2015.

Solveig Walloe, Ulla Vig Nissen, Rune W Berg, Jorn Hounsgaard, and Bente Pakkenberg. Stereological estimate of the total number of neurons in spinal segment D9 of the red-eared turtle. *J. Neurosci.*, 31 (7):2431–5, feb 2011. ISSN 1529-2401. doi: 10.1523/JNEUROSCI.3938-10.2011. URL http://www.ncbi.nlm.nih.gov/pubmed/21325510.

Charles J Wilson and R N S Sachdev. Intracellular and juxtacellular staining with biocytin. *Current protocols in neuroscience*, Chapter 1:Unit 1.12, 2004. ISSN 1934-8576. doi: 10.1002/0471142301.ns0112s26.

Jiwon Woo, Mirae Lee, Jeong Min Seo, Hyo Suk Park, and Yong Eun Cho. Optimization of the optical transparency of rodent tissues by modified PACT-based passive clearing. *Experimental & Molecular Medicine*, 48(12):e274, dec 2016. doi: 10.1038/emm.2016.105. URL https://doi.org/10.1038%2Femm.2016.105.

Anna L. Xavier, Romain Fontaine, Solal Bloch, Pierre Affaticati, Arnim Jenett, Michaël Demarque, Philippe Vernier, and Kei Yamamoto. Comparative analysis of monoaminergic cerebrospinal fluid-contacting cells in osteichthyes (bony vertebrates). *Journal of Comparative Neurology*, 525(9):2265–2283, 2017. ISSN 1096-9861. doi: 10.1002/cne.24204. URL http://dx.doi.org/10.1002/cne.24204.

B Yang, JB Treweek, RP Kulkarni, BE Deverman, CK Chen, E Lubeck, S Shah, L Cai, and V Gradinaru. Single-cell phenotyping within transparent intact tissue through whole-body clearing. *Cell*, 158:945–58, Aug 2014.

T Yu, Y Qi, J Zhu, J Xu, H Gong, Q Luo, and D Zhu. Elevated-temperature-induced acceleration of PACT clearing process of mouse brain tissue. *Sci Rep*, 7:38848, Jan 2017.

H Zheng and L Rinaman. Simplified CLARITY for visualizing immunofluorescence labeling in the developing rat brain. *Brain Struct Funct*, 221:2375–83, May 2016.